CRYSTAL GROWTH & DESIGN

Article

pubs.acs.org/crystal

# Inhibition of Calcite Growth: Combined Effects of $Mg^{2+}$ and $SO_4^{2-}$

M. R. Nielsen,[*,†] K. K. Sand,[†,‡] J. D. Rodriguez-Blanco,[†,#] N. Bovet,[†] J. Generosi,[†] K. N. Dalby,[†] and S. L. S. Stipp[†]

[†]Nano-Science Center, Department of Chemistry, University of Copenhagen, Copenhagen, Denmark

[‡]Physical Sciences Division, Pacific Northwest National Laboratories, Richland, Washington, United States

**ABSTRACT:** Magnesium and sulfate are each known to affect calcite growth and dissolution, but little is known about their combined effects on calcite growth rates. We grew calcite using the constant composition approach at ambient conditions, monitoring inhibition in solutions of $Mg^{2+}$ and $SO_4^{2-}$ individually and together. The growth rate for pure calcite averaged $4.35 \times 10^{-6}$ mol $m^{-2}$ $s^{-1}$ but decreased to 0.34, 0.16, and $0.08 \times 10^{-6}$ mol $m^{-2}$ $s^{-1}$ in solutions with 40 mM of $SO_4^{2-}$, 13.3 mM of $Mg^{2+}$, and 12.7 mM of $MgSO_4$. We characterized the crystal form with scanning electron microscopy and atomic force microscopy. The {10$\bar{1}$0} crystal surface developed as the foreign ion concentration increased in the order $SO_4^{2-}$ < $Mg^{2+}$ < $MgSO_4$. Powder X-ray diffraction and X-ray photoelectron spectroscopy showed Mg incorporation of as much as 9.2 mol %. $Mg^{2+}$ inhibits calcite growth more effectively when $SO_4^{2-}$ is also present, which we interpret to be the result of $MgSO_4$ ion pair formation. Sulfate promotes $Mg^{2+}$ dehydration, thereby allowing calcite uptake at lower temperatures. These results improve general understanding about the controls on biomineralisation and imply a need for re-examining the validity of the Mg/Ca thermometer, which uses the Mg composition in foraminifer for interpreting ancient seawater temperatures.

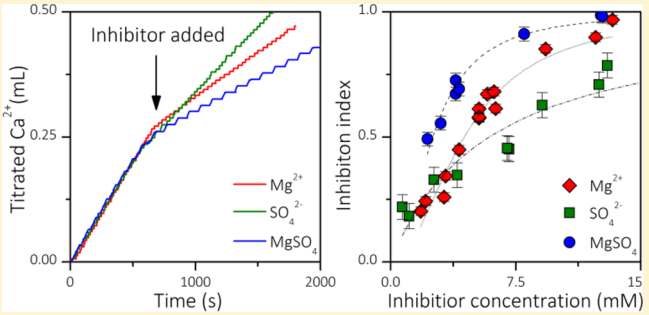


## INTRODUCTION

Calcite is found in nearly all low temperature (<50 °C) natural systems.[1,2] It is common as a biomineral,[3−5] such as in coccolithophores and foraminifera. Carbonate rocks often form from biogenically produced calcite fragments and are often porous, making them common as aquifers for groundwater and reservoirs for gas and oil. Controlling the rates of calcite growth and dissolution is of interest in applications such as the properties of cement, preventing scaling in pipes and manufacture of particles used for pigments, paper, and pharmaceuticals.

It has long been known that calcite readily takes up trace elements such as $F^-$, $Mn^{2+}$, $Co^{2+}$, $Ni^{2+}$, $Zn^{2+}$, $Se^{2-}$, $Sr^{2+}$, $Cd^{2+}$, $Ba^{2+}$, $Eu^{3+}$, and $UO_2^{2+}$.[6−18] The affinity for calcite of many of these elements has been studied individually, but surprisingly little is known about competition or enhancement when multiple ions are present. Trace element immobilization is a benefit for waste storage and for remediation of contaminated soil and water in the environment. Adsorption and incorporation of trace ions and organic compounds on and in calcite can influence rates of growth and dissolution,[19−22] local ion transport,[23] crystal form,[24,25] and surface free energy, i.e., wettability.[26−29] In particular, tuning the wettability of mineral surfaces, such as it long has been used for ore mineral separation, is a promising approach for enhancing oil recovery (EOR). When pore surfaces are made more water wet, oil production increases.[28] Many researchers have studied the role of the common seawater ions $Mg^{2+}$, $Ca^{2+}$, $Na^+$, $K^+$, and $SO_4^{2-}$, for controlling wettability in sandstone and carbonate rocks.[27,30−35]

The behavior of $Mg^{2+}$ and $SO_4^{2-}$ in carbonate rocks is particularly interesting because they are common divalent ions in seawater. Many studies have evaluated the effect of either $Mg^{2+}$ or $SO_4^{2-}$ adsorption. They have been shown to decrease the rates of $CaCO_3$ nucleation and growth, and they modify the crystal form and surface properties.[36−39] The presence of $Mg^{2+}$, particularly when $[Mg^{2+}]_{aq}$ > $[Ca^{2+}]_{aq}$, determines which $CaCO_3$ polymorph dominates, promoting aragonite instead of calcite.[19,29,36,39−43] The inhibition of growth has been explained to result from blocked growth sites,[44,45] from a change in the saturation state[41] and from modified structural instability because of adsorbed foreign ions.[21] In general, the higher the temperature, the greater the incorporation of $Mg^{2+}$,[40,46,47] and this relationship is used as a proxy for interpreting ancient seawater temperature and salinity.[48−50]

A number of authors have studied the combined effect of $Mg^{2+}$ and $SO_4^{2-}$. Experimental work by Sjöbjerg[38] and later Gledhill and Morse[51] revealed that both ions decrease the dissolution rate to a higher degree than $Mg^{2+}$ only. Likewise Mucci et al.[52] found that growth rates for calcite decreased in artificial seawater (ASW) compared with behavior in ASW without $SO_4^{2-}$. When $CaCO_3$ nucleates from solutions with

**Received:** April 7, 2016
**Revised:** September 20, 2016
**Published:** September 26, 2016





DOI: 10.1021/acs.cgd.6b00536
*Cryst. Growth Des.* 2016, 16, 6199−6207

**Table 1. Experimental Conditions for Seeded Calcite Precipitation Experiments**

| | | | | inhibitor concentration (mM) | | | growth rate (mol $m^{-2}$ $s^{-1}$) | | |
|---|---|---|---|---|---|---|---|---|---|
| run | start pH | SI | seed mass (mg) | $Mg^{2+}$ | $SO_4^{2-}$ | $MgSO_4$ | $R_o \times 10^6$ | $R_i \times 10^6$ | Θ |
| Exp. 1 | 8.39 | 1.17 | 29.2 | 1.8 | | | 2.73 | 2.18 | 0.20 ± 0.02 |
| Exp. 2 | 8.30 | 1.07 | 32.5 | 2.1 | | | 5.69 | 4.31 | 0.24 ± 0.02 |
| Exp. 3 | 8.34 | 1.11 | 30.6 | 3.2 | | | 2.36 | 1.75 | 0.26 ± 0.02 |
| Exp. 4 | 8.38 | 1.16 | 30.9 | 3.3 | | | 2.46 | 1.62 | 0.34 ± 0.02 |
| Exp. 5 | 8.34 | 1.11 | 28.2 | 4.1 | | | 5.38 | 2.96 | 0.45 ± 0.02 |
| Exp. 6 | 8.33 | 1.10 | 31.0 | 5.3 | | | 5.03 | 2.11 | 0.58 ± 0.02 |
| Exp. 7 | 8.31 | 1.08 | 30.1 | 5.3 | | | 4.49 | 1.91 | 0.58 ± 0.02 |
| Exp. 8 | 8.32 | 1.09 | 32.8 | 5.3 | | | 4.84 | 1.88 | 0.61 ± 0.02 |
| Exp. 9 | 8.30 | 1.07 | 31.4 | 5.3 | | | 4.76 | 2.00 | 0.58 ± 0.02 |
| Exp. 10 | 8.40 | 1.18 | 30.1 | 5.8 | | | 2.50 | 0.82 | 0.67 ± 0.02 |
| Exp. 11 | 8.37 | 1.14 | 30.5 | 6.2 | | | 2.34 | 0.74 | 0.68 ± 0.02 |
| Exp. 12 | 8.29 | 1.06 | 29.2 | 6.3 | | | 5.23 | 2.02 | 0.61 ± 0.02 |
| Exp. 13 | 8.31 | 1.08 | 30.1 | 9.3 | | | 5.33 | 0.79 | 0.85 ± 0.02 |
| Exp. 14 | 8.32 | 1.09 | 29.7 | 12.3 | | | 5.16 | 0.52 | 0.90 ± 0.02 |
| Exp. 15 | 8.30 | 1.07 | 30.3 | 13.3 | | | 4.98 | 0.16 | 0.97 ± 0.02 |
| Exp. 16 | 8.31 | 1.08 | 29.5 | | 0.70 | | 4.89 | 3.82 | 0.22 ± 0.05 |
| Exp. 17 | 8.30 | 1.07 | 29.0 | | 1.1 | | 4.63 | 3.78 | 0.18 ± 0.05 |
| Exp. 18 | 8.31 | 1.08 | 30.0 | | 2.6 | | 4.97 | 3.33 | 0.33 ± 0.05 |
| Exp. 19 | 8.31 | 1.08 | 28.8 | | 4.0 | | 4.49 | 2.93 | 0.35 ± 0.05 |
| Exp. 20 | 8.40 | 1.18 | 30.9 | | 7.0 | | 2.59 | 1.41 | 0.46 ± 0.05 |
| Exp. 21 | 8.27 | 1.04 | 30.1 | | 7.1 | | 4.01 | 2.20 | 0.45 ± 0.05 |
| Exp. 22 | 8.33 | 1.10 | 30.5 | | 9.1 | | 4.79 | 1.79 | 0.63 ± 0.05 |
| Exp. 23 | 8.30 | 1.07 | 32.0 | | 12.5 | | 4.78 | 1.39 | 0.71 ± 0.05 |
| Exp. 24 | 8.30 | 1.07 | 29.9 | | 13.0 | | 5.79 | 1.24 | 0.79 ± 0.05 |
| Exp. 25 | 8.29 | 1.06 | 29.1 | | 20.5 | | 5.08 | 1.13 | 0.78 ± 0.05 |
| Exp. 26 | 8.31 | 1.08 | 31.0 | | 40.0 | | 4.54 | 0.34 | 0.93 ± 0.05 |
| Exp. 27 | 8.31 | 1.08 | 31.40 | | | 0.14 | 4.79 | 3.24 | 0.32 ± 0.03 |
| Exp. 28 | 8.31 | 1.08 | 30.6 | | | 2.2 | 3.84 | 1.95 | 0.49 ± 0.03 |
| Exp. 29 | 8.30 | 1.07 | 29.5 | | | 3.0 | 3.17 | 1.41 | 0.56 ± 0.03 |
| Exp. 30 | 8.32 | 1.09 | 30.1 | | | 3.9 | 4.00 | 1.09 | 0.73 ± 0.03 |
| Exp. 31 | 8.32 | 1.09 | 33.0 | | | 3.9 | 4.38 | 1.44 | 0.67 ± 0.03 |
| Exp. 32 | 8.32 | 1.09 | 30.6 | | | 4.1 | 4.37 | 1.35 | 0.69 ± 0.03 |
| Exp. 33 | 8.33 | 1.10 | 31.3 | | | 8.0 | 3.85 | 0.34 | 0.91 ± 0.03 |
| Exp. 34 | 8.31 | 1.08 | 30.6 | | | 12.6 | 5.73 | 0.08 | 0.99 ± 0.03 |
| Exp. 35 | 8.31 | 1.08 | 32.2 | | | 12.7 | 4.83 | 0.08 | 0.98 ± 0.03 |
| Exp. 36 | 8.30 | 1.07 | 30.0 | | | | 4.64 | | |
| Exp. 37 | 8.30 | 1.07 | 60.0 | 10 | | | 4.71 | | |
| Exp. 38 | 8.29 | 1.06 | 60.1 | | | 10 | 4.70 | | |

$Mg^{2+}$ and $SO_4^{2-}$, the induction time increases[53] and causes severe modifications in crystal forms.[42,54,55] Calcite composition also changed in the presence of these two ions, but reports are contradictory. Both Kralj et al.[42] and Falini et al.[56] reported that the amount of Mg that is structurally incorporated into calcite was enhanced by $SO_4^{2-}$, but Mucci et al.[52] reported the opposite effect for calcite in ASW. Experimental work so far has been conducted using solution mixing and constant addition approaches, where the initial conditions have been far from equilibrium. Thus, the reaction rates and the influence of trace elements on crystal properties from these studies do not represent most systems in nature. Experiments to investigate the effect of pore fluid composition on the release of oil showed that pore surfaces in limestone became more water wet, especially at temperatures >70 °C, when both $Mg^{2+}$ and $SO_4^{2-}$ were present.[27] Molecular modeling by Sakuma et al.[29] explained why. Mg substitution for Ca in calcite is favored when $SO_4^{2-}$ is also present, leading to a more water wet surface.

We wanted to experimentally test the results of Sakuma et al.[29] For this purpose we used a constant composition approach, where pH and saturation index (SI) were held constant, so we could (i) quantify growth rates, (ii) evaluate $Mg^{2+}$ and $SO_4^{2-}$ incorporation, and (iii) investigate surface changes during calcite growth. The solids were then characterized by powder X-ray diffraction (PXRD), X-ray photoelectron spectroscopy (XPS), scanning electron microscopy (SEM), and atomic force microscopy (AFM).

## MATERIALS AND METHODS

All solutions were prepared with ultrapure deionized water (Milli-Q, resistivity >18.2 MΩ·cm) with compounds from Sigma-Aldrich ($CaCl_2 \cdot 2H_2O$, NaCl, $MgSO_4 \cdot 7H_2O$, $Na_2SO_4$, and $NaHCO_3$; purity 99.7%) and Merck P.A. ($Na_2CO_3$, $MgCl_2 \cdot 6H_2O$). All were reagent grade or better. Cation concentrations in the starting solutions were confirmed with atomic absorption spectrometry (AAS, PerkinElmer AAS Analyst 800). Merck calcite (>99.9% purity) was used as seed. Prior to use, the calcite powder was recrystallized in ultrapure water that was bubbled with $CO_2$ at 60 °C through several cycles, using a method adapted from Stipp and Hochella[57] to remove organic compounds added during the commercial synthesis. On the treated material, the BET surface area was determined to be 0.31 $m^2/g$, using a



DOI: 10.1021/acs.cgd.6b00536
Cryst. Growth Des. 2016, 16, 6199−6207

Quantachrome Autosorb-1 Sorption analyzer, X-ray diffraction proved no phases in the seed other than calcite, and scanning electron microscopy (SEM) images showed particles with typical dimensions of 30 $\mu$m and a homogeneous size distribution.

Constant composition experiments were carried out using the apparatus developed and described by Lakshtanov et al.[58] We used a double-walled glass reaction vessel, maintained at 25 ± 0.1 °C and stirred at ∼300 rpm with an overhead propeller (Metrohm 802). A volume of 35 mL solution was prepared to have a final concentration of 4.0 mM $CaCl_2$, 4.0 mM $NaHCO_3$, and 0.1 M NaCl (ionic strength, IS = 0.1 M); it was filtered (0.22 $\mu$m pore size) and added to the reaction vessel. If needed, the solution pH was adjusted to 8.3 ± 0.1 with a few drops of 0.05 M HCl. This solution was supersaturated with respect to calcite. The saturation index, with respect to calcite, $SI_{cc}$, was 1.0, determined using the geochemical speciation code PHREEQC:[59]

$$SI_{cc} = \log \frac{[Ca^{2+}][CO_3^{2-}]}{K_{sp(cc)}} \quad (1)$$

where $[Ca^{2+}]$ and $[CO_3^{2-}]$ represent the ion activities of calcium and carbonate and $K_{sp(cc)}$ represents the solubility product of calcite,[60] namely, $10^{-8.48}$.

The experiment began when 30 ± 4 mg of calcite seed was added to the solution. Calcite precipitated by the reaction:

$$Ca^{2+} + HCO_3^- \leftrightarrow CaCO_{3(s)} + H^+ \quad (2)$$

As calcite formed, the concentration of $Ca^{2+}$, $HCO_3^-$, and pH decreased. The change in pH triggers addition of equal volumes of 0.1 M $CaCl_2$ and 0.1 M $Na_2CO_3$, which returns pH to the initial value (8.3 ± 0.02). After 15 min of undisturbed growth of pure calcite, a specific volume of $MgCl_2$ or $Na_2SO_4$ or $MgSO_4$ solution was added. Volumes of the solutions ranged from 0.150 to 5.00 mL, and concentrations ranged from 0.1 to 0.5 M, yielding final concentrations that ranged from 0.7 to 40 mM. We allowed precipitation to continue for 30 min more. Table 1 (left side) lists the conditions of the experiments. Experiment 36 was the control, with only calcite.

Within a minute of adding solutions containing $MgCl_2$, $Na_2SO_4$, or $MgSO_4$, we took a 300 $\mu$L sample of growth solution. Another sample was taken 30 min later, at the end of the experiments. The solutions were filtered, and the liquid was analyzed by AAS and ion chromatography (IC, Metrohm 861 Advanced compact IC) to determine the concentrations of $Ca^{2+}$, $Mg^{2+}$ (AAS), and $SO_4^{2-}$ (IC). The solids were rinsed with ethanol to remove the last of the solution to minimize precipitation, dried in air, and stored for later analysis. Ethanol has been shown to displace water and to remain attached to the calcite surface, thus inhibiting recrystallization, also in the absence of liquid water.[20,61,62] The titrated volumes of $CaCl_2$ and $Na_2CO_3$ were recorded automatically and used to determine growth rate using the expression:

$$R = \frac{[Ca^{2+}]_{titrant}}{m_{seed} SA_{seed}} \frac{dV}{dt} \quad (3)$$

where $[Ca^{2+}]_{titrant}$ represents the concentration of $Ca^{2+}$ in the titrant $CaCl_2$ solution, $m_{seed}$, the initial seed mass, $SA_{seed}$, the specific surface area of the seed, and $dV/dt$, the volume added per unit time. Because the surface area increase during growth is so small, the assumption of constant surface area in the equation is considered valid. In total, we carried out 38 experiments. Figure 1 illustrates data from a typical example. To quantify the degree of inhibition, we determined the inhibition index, Θ, which relates the undisturbed growth rate, i.e., rate in the pure calcite system, $R_0$, to the growth rate in the solution containing the inhibitor, $R_i$:

$$\Theta = \frac{R_0 - R_i}{R_0} \quad (4)$$

When growth completely stops, Θ = 1. The results for all of the experiments are presented in Table 1, right side.

The initial seed material and the solids removed at the end of the experiments with $Mg^{2+}$, $SO_4^{2-}$, and $MgSO_4$, at concentrations ranging from ∼2 mM to ∼13 mM, were analyzed quantitatively by PXRD to verify their mineral composition. For control, we also analyzed a sample from the pure system (Experiment 36). In the samples that contained Mg, the character of the Mg calcite was determined using the following expression after Arvidson and Mackenzie[63]

$$X_{(MgCO_3)} = -3.6393 d_{(10\bar{1}4)} + 11.0405 \quad (5)$$

where $X_{(MgCO_3)}$ represents the mole percent $MgCO_3$ in the calcite and $d_{(10\bar{1}4)}$ represents the peak intensity in Å.

For X-ray diffraction (XRD), we used a Bruker D8 Discover (CoK$\alpha_1$, 1.7902 Å; 2$\theta$ range 5−90; 0.01°/step and 0.1 s/step). Structural parameters were estimated from the diffraction patterns using the Scherrer equation,[64] with the assumption that the particles were stress free. The pattern matching refinement of the data for the crystalline phases was carried out using the Rietveld refinement software, TOPAS.[65] We used a silicon standard ($2\theta_{111}$ = 28.46°; fwhm = 0.049°).

We also analyzed the solids with X-ray photoelectron spectroscopy (XPS). This technique provides information about the elements that are present and how they are bound to other elements, from the top 10 nm of a solid. We used a Kratos AXIS Ultra$^{DLD}$ instrument, with monochromatic $Al_{K\alpha}$ X-rays ($h\nu$ = 1486.6 eV; power = 150 W). The pass energy for wide scans was 160 eV, and for high resolution scans, it was 20 eV. Data were analyzed with CasaXPS software, using the C 1s peak for $CO_3$ at 290.1 eV for energy calibration.[57] The position, width, and intensity of the various peaks were examined with XPS on samples collected at the beginning and end of the experiments. There was no detectable evidence of X-ray beam damage on surface composition.

We collected scanning electron microscopy (SEM) images of the solids at the micrometer scale using a Quanta 3D FEG 200/600 SEM, in high vacuum ($5 \times 10^{-4}$ Pa), with an acceleration voltage of 2.00 kV and a beam current of 16.6 pA. All samples were uncoated and fixed to double sided carbon tape on stainless steel holders. Atomic force microscopy (AFM) images were collected to monitor the change in surface form at sub-micrometer scale using an Asylum Research MFP-3D AFM. Olympus AC240TS silicon cantilevers, with a nominal spring constant of 2 N/nm, were used in AC mode, in air at room temperature to produce topography images.

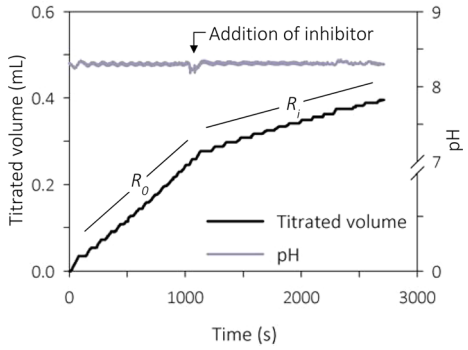


**Figure 1.** Volume of titrant added and pH in the growth solution for Experiment 10, where we added 5.8 mM $MgCl_2$ at the time indicated by the arrow. Growth rate before ($R_0$) and after ($R_i$) inhibitor addition is derived from the slope of the lines.

## RESULTS AND DISCUSSION

Calcite growth is influenced by the presence of $SO_4^{2-}$, $Mg^{2+}$, and $MgSO_4$ but to different extents. Figure 2 shows the inhibition index, Θ, as a function of additive concentration. All results are presented numerically on the right side of Table 1.

Inhibition increased with concentration in the order $MgSO_4$ > $Mg^{2+}$ ≫ $SO_4^{2-}$. In particular, at 12.6 mM $MgSO_4$, the inhibition index reached 0.99, compared with 0.90 and 0.71 for similar concentrations of $Mg^{2+}$ and $SO_4^{2-}$ alone. To reach an inhibition index above 0.9 for $SO_4^{2-}$, a significantly higher


DOI: 10.1021/acs.cgd.6b00536
Cryst. Growth Des. 2016, 16, 6199−6207

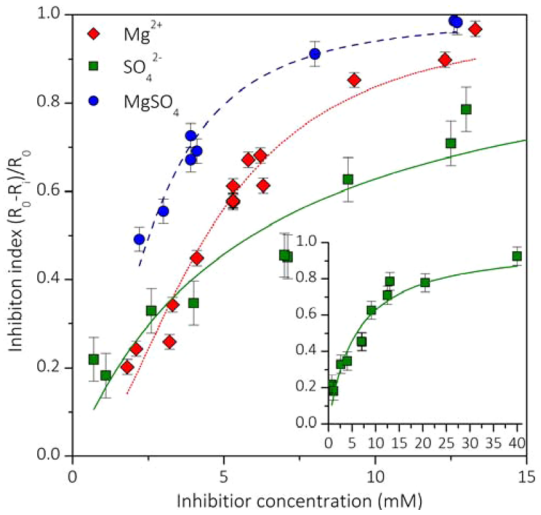


**Figure 2.** Inhibition index, Θ, as a function of the concentrations of $Mg^{2+}$, $SO_4^{2-}$, and $MgSO_4$. Fit lines correspond to a first-order Langmuir equation for $SO_4^{2-}$ and a second order Langmuir equation for $Mg^{2+}$ and $MgSO_4$. Inserted is the full concentration range for $SO_4^{2-}$.

concentration was needed. For example, at 40 mM $SO_4^{2-}$, Θ = 0.92. We tested the dependence of the inhibition index on concentration. The $SO_4^{2-}$ results could be described by a first-order Langmuir adsorption model. The fit was good ($R^2$ = 0.92), suggesting that the formation of a monolayer of $SO_4^{2-}$ ions, adsorbed at growth sites, blocks further growth. This is comparable to results by Amjad et al.,[66] who observed a similar behavior for polyphosphate on hydroxyapatite in constant composition experiments. The fits for $Mg^{2+}$ and $MgSO_4^{2-}$ with a first order Langmuir model were poor ($R^2$ = 0.78 and $R^2$ = 0.83), but with a second order Langmuir curve, they were quite good ($R^2$ = 0.97 and $R^2$ = 0.96). This indicates that the mechanism for growth inhibition is more complex than simple adsorption and site blocking, for which our XPS and XRD results provide insight.

Our observed decrease in growth rate with $MgSO_4$ in the near equilibrium, constant composition system is similar to the results of Mucci et al.[52] and Mejri et al.[40] who studied growth rates in free drift systems that were more supersaturated than ours. Mucci et al.[52] found a 2−3 fold decrease in calcite precipitation rate in artificial seawater (ASW) compared with rates in ASW that did not contain $SO_4^{2-}$. Mejri et al.[40] reported a decrease in growth rate caused by $Mg^{2+}$ or $SO_4^{2-}$ during homogeneous $CaCO_3$ precipitation and Gledhill and Morse,[51] reported that the extent of $SO_4^{2-}$ inhibition on calcite growth is sensitive to the concentrations of $Ca^{2+}$ and $Mg^{2+}$.

XPS showed clear evidence of $Mg^{2+}$ and/or $SO_4^{2-}$ within the top 10 nm of calcite grown in the single and the double ion solutions (Table 2) with the peak for Mg 2s at 89.6 ± 0.1 eV and for S 2p3/2 at 169.5 ± 0.1 eV. Evidence of surface $Mg^{2+}$ and/or $SO_4^{2-}$ supports our interpretations of the Langmuir fitting. A control sample from a pure system (Experiment 36) showed no traces of these ions.

From the amount of Ca that we added in the constant composition set up, we could determine the amount taken up to form the new calcite, and thus we could calculate the number of calcite unit cells grown during the inhibited stage. We estimated that the newly precipitated material would form a layer equivalent to >30 nm if it precipitated uniformly over the seeds. We do not know how the new material distributed itself, but we assumed that our XPS analyses, with a maximum information depth of 10 nm, represent the elemental composition of the newly precipitated phase, not the underlying seed crystals.

The $CO_3$/Ca ratio from the XPS data for pure calcite is not 1:1, as one might expect from the atomic proportions in the bulk mineral because the surface composition reflects interactions (relaxation and hydration) resulting from termination of the bulk calcite structure.[57] We see this reflected in the composition of the pure system where the peak intensity ratio for $CO_3$/Ca is 0.87 (Experiment 36, Table 2). The ratio is 0.83 for the sample that grew in the presence of $SO_4^{2-}$ (Experiment 24), which is close to the pure calcite system ratio but reflects adsorption of $SO_4$ and some substitution for surface $CO_3$. $SO_4$ uptake is consistent with observations by others.[39,67−71] However, because the decrease of the ratio is so small and the $SO_4^{2-}$ growth inhibition data follow a first-order Langmuir isotherm, we interpret that $SO_4$ uptake into the bulk is not significant when $SO_4^{2-}$ is the only ion. In solutions that contain $Mg^{2+}$ alone, the $CO_3$/Ca ratio increases to 0.92 or more, which is consistent with constant $CO_3$ and lower Ca, implying substitution by Mg. For solutions with $MgSO_4$, the $CO_3$/Ca ratio increases further to 0.98 for the 12.6 mM $MgSO_4$ solution (Experiment 34 in Table 2).

**Table 2. XPS Results and Calculated Calcite Composition**[a]

| | inhibitor concentration (mM) | | | | | | | |
|---|---|---|---|---|---|---|---|---|
| run | $Mg^{2+}$ | $SO_4^{2-}$ | $MgSO_4^{2-}$ | Mg (atom %) | S ($SO_4^{2-}$) (atom %) | Mg/Ca | $CO_3$/Ca | Mg 1s/Mg 2s |
| Exp. 36 | | | | 0.0 | 0.0 | 0.00 | 0.87 | |
| Exp. 24 | | 13.0 | | 0.0 | 1.0 ± 0.05 | 0.00 | 0.83 | |
| Exp. 37a | 10.0 | | | 5.2 ± 0.3 | 0.0 | 0.03 | 0.92 | 8.27 |
| Exp. 37b | 10.0 | | | 6.7 ± 0.3 | 0.0 | 0.07 | 0.93 | 4.51 |
| Exp. 37b | 10.0 | | | 6.4 ± 0.3 | 0.0 | 0.07 | 0.92 | 4.46 |
| Exp. 15 | 13.3 | | | 9.3 ± 0.5 | 0.0 | 0.13 | 0.96 | 3.86 |
| Exp. 27 | | | 0.14 | 0 | 0 | 0 | 0.86 | |
| Exp. 38a | | | 10.0 | 5.9 ± 0.3 | 0.4 ± 0.02 | 0.03 | 0.91 | 11.07 |
| Exp. 38b | | | 10.0 | 6.4 ± 0.3 | 0.5 ± 0.03 | 0.07 | 0.93 | 4.55 |
| Exp. 38b | | | 10.0 | 5.2 ± 0.3 | 0.6 ± 0.03 | 0.07 | 0.92 | 3.98 |
| Exp. 34 | | | 12.6 | 12.6 ± 0.6 | 0.5 ± 0.02 | 0.16 | 0.98 | 3.96 |

[a]In the sample numbers, a refers to the initial sampling event, within 3 min of adding the inhibitor, and b refers to the sample from the end of the experiment. Two samples (37b and 38b) were analyzed at two separate spots to demonstrate sample homogeneity.



DOI: 10.1021/acs.cgd.6b00536
Cryst. Growth Des. 2016, 16, 6199−6207

The width of the XPS peaks provides information about the types of atomic environment.[72] In Figure 3 Experiment 36

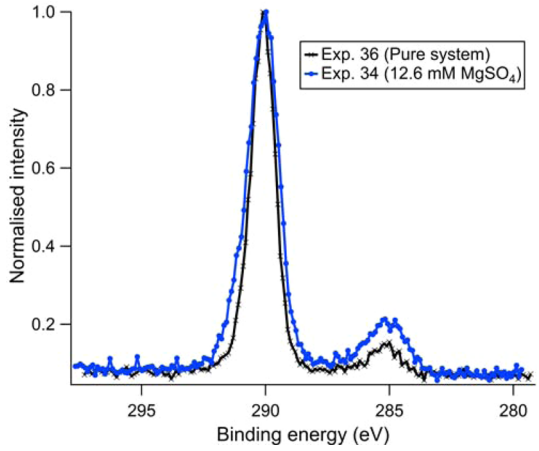


**Figure 3.** High resolution XPS spectra of the C 1s region for Experiments 34 and 36. The most intense peak at 190.1 eV results from C in carbonate bonds.[72] The peak near 285 eV represents adventitious carbon. The fwhm of the carbonate peak is wider for the sample exposed to MgSO4 (1.5 eV) than the pure system (1.2 eV) because there are more environments for C in the mixed carbonate phase.

(pure $CaCO_3$ system) and Experiment 34 (12.6 mM $MgSO_4$) are presented. For the pure system, all C atoms in carbonate ions are in the same environment with O surrounding them. The full width at half-maximum (fwhm) for the C 1s peak that is attributed to carbonate was narrow, 1.20 ± 0.05 eV. For the highest $MgSO_4$ concentration (12.6 mM, Experiment 34), fwhm was 0.3 eV wider, 1.50 ± 0.05 eV. This indicates more than one local environment around carbon, which can be explained by the slight difference in bond distance for $CO_3$ to Mg and $CO_3$ to Ca. The widened peak is really a superposition of two peaks to represent the two different C environments. The Ca 2p peaks also broadened, from 1.50 ± 0.05 eV for pure calcite to 1.65 ± 0.05 eV for the product of Experiment 34. This broadening represents several bonding environments around the Ca ions as a result of the presence of Mg and $SO_4$.

A rough estimate for the composition of the outer layer of newly formed calcite, based on the Mg/Ca ratio, gives $Ca_{0.86}Mg_{0.14}CO_3$ for the two samples formed from the most concentrated solutions. The Mg/Ca ratio includes contributions from both the Mg adsorbed on the calcite surface and Mg that has been incorporated into the near surface.

Two samples each, from Experiment 37 with 10 mM $Mg^{2+}$ and Experiment 38 with 10 mM $MgSO_4$, that were extracted ~2 min after addition of the inhibitor and at the end of the experiment 30 min later, provided insight into the uptake evolution. The Mg 1s/Mg 2s ratio gives information about the relative amount of Mg on and in the near surface at these two time snapshots. The Mg 1s peak results from electrons that are emitted from the first atomic orbital. Their kinetic energy, 182 eV, shows that they are tightly bound in the atom. The Mg 2s peak, generated by electrons from the second atomic orbital, have kinetic energy of 1397 eV, meaning they are much less tightly bound, and when ejected, their higher kinetic energy allows them to escape from deeper within the near surface. Thus, the lower Mg 1s/Mg 2s ratio for the samples collected at the second sampling event, marked "b" in Table 2, indicates that there is more Mg deeper in the near surface, after about 30 min of calcite growth with $Mg^{2+}$ present, as we would expect during continued growth of new Mg calcite. Thus, the $CO_3$/$Ca^{2+}$ ratio difference and the Mg peak broadening indicate that Mg is incorporated into the growing calcite crystal, where it substitutes for Ca. This happens at room temperature, and uptake increases as solution $Mg^{2+}$ concentration increases.

XRD confirmed that all samples consisted of calcite. The patterns from the samples, taken from solutions where inhibitors were added, were identical to the control calcite sample grown in the pure system (Figure 4), showing the same

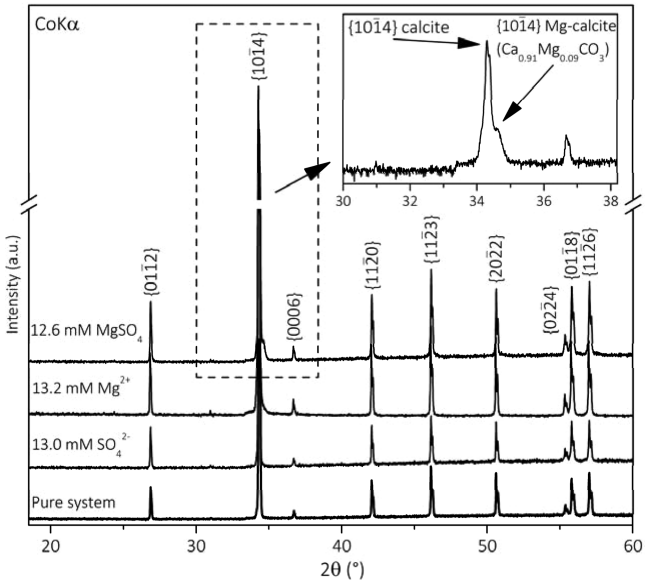


**Figure 4.** X-ray diffraction (XRD) patterns for the calcite samples from the high inhibitor concentration experiments. Inset: Detail of the {10$\bar{1}$4} calcite peak for the final sample taken from Experiment 34 with 12.6 mM $MgSO_4$.

unit cell parameters as pure calcite ($a$ = 4.9896 Å, $c$ = 17.061 Å). For nearly all of the samples, the inclusion of Mg was too low to produce a visible change in the average cell parameters, but this is expected because the 30 nm overlayer of Mg calcite would be swamped in the bulk solid where the pure seed calcite dominates by mass.

The only exception was the 12.6 mM $MgSO_4$ sample (Experiment 34), where the presence of Mg calcite could be seen. We calculated the mole percent of $MgCO_3$ to be ~9.2 mol % (±1 mol %) using the expression presented by Arvidson and Mackenzie,[63] which agrees reasonably well with ~14 mol % (±1 mol %) estimated from the XPS data. The difference between these two results is expected because XPS measures only 10 nm of the near surface, meaning that the inner part of the seed crystals does not influence the measurement. However, XPS does not allow us to differentiate between the Mg that is adsorbed *on* calcite and that which is incorporated *in* the crystal. Adsorbed Mg is undetectable with XRD; only that incorporated in a solid solution has an effect on the peak width. For the other samples, where solutions contained lower concentrations of $Mg^{2+}$, uptake in the near surface was observed by XPS (Table 2), but we could not see Bragg peak shifts, presumably because the dominant {10$\bar{1}$4} calcite peak masks the {10$\bar{1}$4} Mg-calcite peak, which is very close. Mg incorporation at lower concentrations than used in our studies


DOI: 10.1021/acs.cgd.6b00536
Cryst. Growth Des. 2016, 16, 6199−6207

has been identified by Krajl et al.[42] They observed an uptake of 7.5 and 6.3 mol % from solutions with 10 and 5 mM $Mg^{2+}$ in mixing solution experiments. They also reported that the amount of Mg incorporated in the $CaCO_3$ crystals grown from supersaturated solutions varied with the electrolyte anion. $SO_4^{2-}$ led to the highest degree of incorporation, followed by $NO_3^-$ and $Cl^-$.

SEM images show the change in crystal form caused by the inhibitors. Figure 5a shows calcite from the pure system for reference. Terraces are flat and edges and corners are sharp. Change was smallest in the $SO_4^{2-}$ system, higher for $Mg^{2+}$, and highest in the $MgSO_4$ system. The presence of $SO_4^{2-}$ had minimal influence on crystal shape when the concentration was 13 mM (Figure 5b), but $Mg^{2+}$ enhanced the frequency of growth steps, producing rougher terraces and rounded steps (Figure 5c). This was even more pronounced for samples from experiments with $MgSO_4$ solutions (Figure 5d), where the $\{10\bar{1}0\}$ surface also developed. In mixing solution, homogeneous nucleation experiments with $MgSO_4$, Krajl et al.[42] observed $\{01\bar{1}1\}$ surfaces and polycrystalline aggregates. We did not expect to see such behavior in our constant composition experiments, where overgrowth is controlled by the atomic structure of the seed material. Heterogeneous precipitation also explains the absence of aragonite in our experiments with high $Mg^{2+}$ concentrations.

AFM images provided a consistent picture of terrace and step edge topography at higher resolution than SEM images (Figure 6). Calcite surfaces grown in the presence of $SO_4^{2-}$ were least affected (Figure 6a,b). Steps were more rugged than on calcite from a pure system, and there were only a few pits in the terraces (white arrows). In the presence of $Mg^{2+}$ (Figure 5c,d), terraces were irregular and blocky, with wavy edges, and pits were deeper and wider than when the solution contained only $SO_4^{2-}$. The rhombohedral symmetry of the calcite is reflected in pit shape (thick black horizontal arrow in Figure 6d), where the pit edges are pinned and the corners that are produced by intersection of obtuse sides are rounded (Figure 6d white "o"). This is characteristic of growth and dissolution in solutions when $Mg^{2+}$ is present.[19,73] In the $MgSO_4$ solution (Figure 6e and f), the density of pits increased, and they were small and irregular. The terrace edges were also very irregular, suggesting abundant inhibited sites.

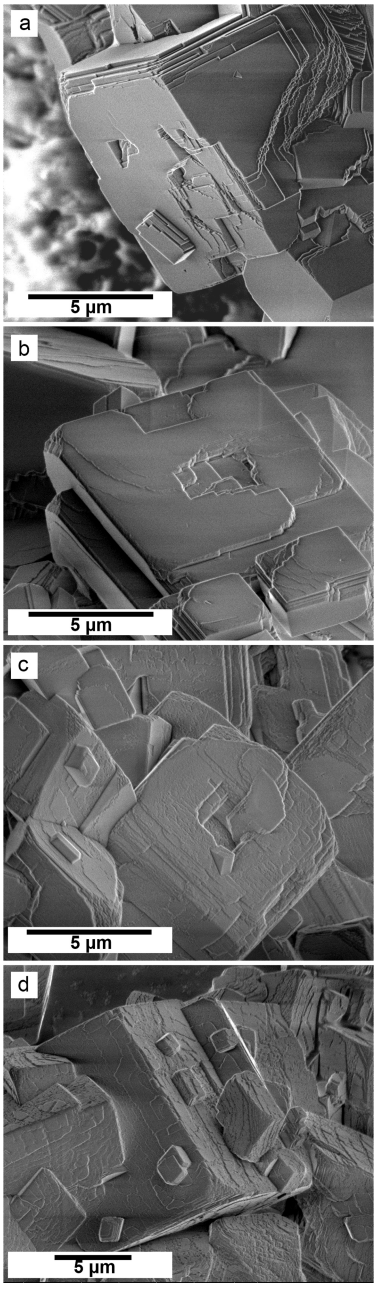


**Figure 5.** Typical scanning electron microscopy (SEM) images of calcite (a) grown without inhibitor and (b) with 13.0 mM $SO_4^{2-}$, (c) 13.2 mM $Mg^{2+}$, and (d) 12.6 mM $MgSO_4$.

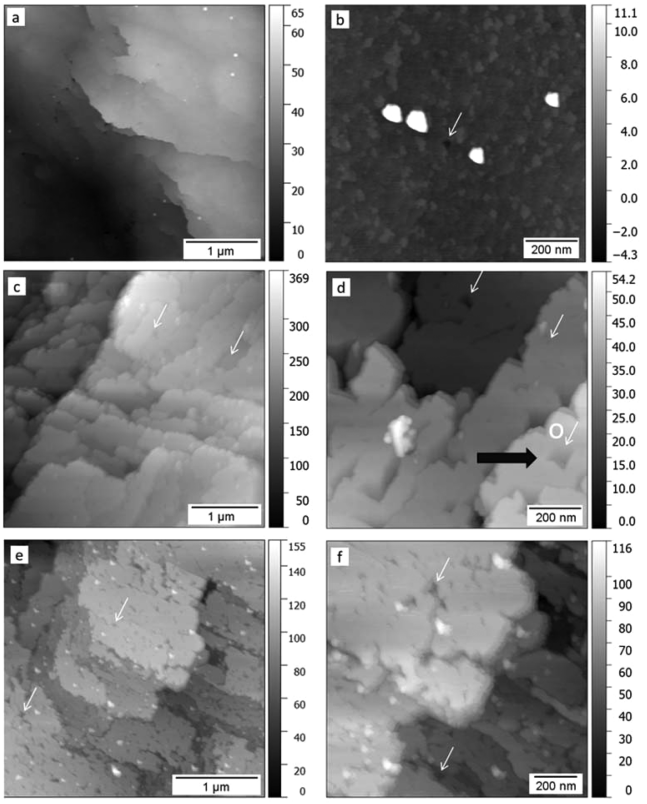


**Figure 6.** Representative atomic force microscopy (AFM) images of calcite (a) and (b) grown with 13.0 mM $SO_4^{2-}$, (c, d) 13.2 mM $Mg^{2+}$, and (e, f) 12.6 mM $MgSO_4$. Thin white arrows indicate pits. In (d) a pit that is rounded at the obtuse corner (marked o) is indicated by a thick black arrow.



DOI: 10.1021/acs.cgd.6b00536
Cryst. Growth Des. 2016, 16, 6199−6207

To quantify the degree of edge roughness, we estimated step irregularity along the crystal edges from AFM images. This parameter compared the real length of an edge over a displacement of 1 $\mu$m with the actual tortuous edge. We made at least three estimates for each sample taken from experiments with the highest inhibitor concentrations, and we averaged the outcome for each system. The resulting irregularity was 1.07 for the sample grown with $SO_4^{2-}$ present, 1.11 for $Mg^{2+}$ and 1.43 for $MgSO_4$, consistent with the qualitative observations from SEM and AFM images.

From the results of this study, it is clear that inhibition caused by $SO_4$ is purely the result of adsorption. This is justified by the uptake data being well described by a first-order Langmuir equation, XRD patterns that revealed nothing but pure calcite, and XPS peak intensity ratios that showed only minor changes in the $CO_3$/Ca ratio. Inhibition in the $Mg^{2+}$ and $MgSO_4$ experiments resulted from two processes: (i) adsorption of Mg (and $SO_4$) and (ii) structural incorporation of Mg during growth.

$Mg^{2+}$ inhibition of calcite precipitation and dissolution is well-known,[36,37,41,42,44,74,75] and our SEM and AFM data are consistent with published reports.[19,42,73,76,77] The electron configuration of $Mg^{2+}$ makes it prone to hydrate, thereby delaying growth in its vicinity.[47,78]

The strongest inhibition occurs when both $Mg^{2+}$ and $SO_4^{2-}$ are present; i.e., $SO_4^{2-}$ enhances the inhibiting effect of $Mg^{2+}$. This is consistent with our observation that in experiments with $MgSO_4$, the calcite form is most affected (irregularity measurement of 1.43) compared with samples from experiments with the individual ions (irregularity for $SO_4^{2-}$: 1.07 and $Mg^{2+}$: 1.11). The mechanism for increased calcite inhibition by $Mg^{2+}$ with $SO_4^{2-}$, proposed by Kralj et al.,[42] suggested that $SO_4^{2-}$ helps dehydrate $Mg^{2+}$ through ion pairing. Sakuma et al.[29] used molecular modeling to show that the substitution of the $MgSO_4$ ion pair into the calcite surface is energetically favored over substitution of pure $Mg^{2+}$. Our results indicate that Mg incorporation is enhanced at ambient conditions when $SO_4^{2-}$ is present, which means that calcite can take up Mg even at room temperature if $SO_4^{2-}$ is also present in solution.

Higher temperature is known to increase the rate and extent of Mg incorporation into bulk $CaCO_3$.[40,46,47] Our results imply that when $SO_4^{2-}$ is present, increased temperature is less necessary, which is interesting information to add to overall understanding of the controls on biomineralisation. It is also useful for the design of specific calcite powders for industrial applications. Better understanding of the uptake of trace components and their effect on wetting properties is useful for enhancing oil recovery and probably also for contaminated groundwater remediation. Affecting the adhesion properties on surfaces provides inspiration for preventing scaling in that the effectiveness of the known inhibitor, magnesium, can be improved by adding sulfate. The new insight is useful for controlling calcite wettability, growth rate, crystal size, shape, and surface character. Confirmation that magnesium uptake is enhanced by sulfate implies a need to re-examine the validity of the Mg/Ca thermometer for foraminifera and its application for interpreting ancient seawater temperatures.

## CONCLUSIONS

The presence of $Mg^{2+}$ and $SO_4^{2-}$, individually and together, influenced calcite crystal shape and roughness. Solutions containing both $Mg^{2+}$ and $SO_4^{2-}$ promoted the greatest disruption, resulting in rough edges and pitted terraces. All three ions inhibited calcite growth in the order $SO_4^{2-} \ll Mg^{2+} < MgSO_4$, proportional to their concentrations. $SO_4^{2-}$ is the weakest inhibitor. It adsorbs to surfaces and blocks growth sites. $Mg^{2+}$ adsorbs and is incorporated into the growing mineral. The effect of magnesium is enhanced, when $SO_4^{2-}$ is also present.

## AUTHOR INFORMATION


### Corresponding Author

*Address: Nano-Science Center, Department of Chemistry, University of Copenhagen, Universitetsparken 5 DK-2100, Copenhagen, Denmark. Phone: +4530427032. E-mail: rnielsen@nano.ku.dk.

### Present Address

#Department of Geology, Trinity College Dublin, Dublin 2, Ireland.


### Notes

The authors declare no competing financial interest.

## ACKNOWLEDGMENTS

We sincerely thank K. West, L. Lakshtanov, D. Okhrimenko, S. Dobberschütz, and the NanoGeoScience Group members for discussion. We are grateful to three anonymous reviewers. Funding was provided by the UK Engineering and Physical Sciences Research Council [EPSRC Grant Number EP/I001514/1], through the Materials Interface with Biology (MIB) Consortium. This study was affiliated with the Mineral Scaling (MINSC) ITN, funded by the European Commission [Grant Agreement No: FP7-290040]. K.K.S. is grateful for funding from the Danish Council for Independent Research on their Individual Post Doc (0602-02915B) and Sapere Aude Programs (0602-02654B). J.D.R.-B. acknowledges the financial support by the NanoCArB (PIEF-GA-2013-624016) Marie Curie Intra-European Fellowship (IEF). The project was made possible by access to instruments funded by Maersk Oil and Gas A/S.

## REFERENCES


(1) Millero, F. J. *Chemical Oceanography*; CRC Press: Boca Raton, FL, 1996.

(2) Morse, J. W.; Mackenzie, F. T. *Geochemistry of Sedimentary Carbonates*; Elsevier: Amsterdam, 1990.

(3) Mann, S. *Biomineralization, Principles and Concepts in Bioinorganic Materials Chemistry*; Oxford University Press: Oxford, 2001.

(4) Meldrum, F. C.; Colfen, H. *Chem. Rev.* **2008**, *108* (11), 4332−4432.

(5) Bauerlein, E. *Handbook of Biomineralization: Biological Aspects and Structure Formation*; Wiley-VCH Verlag GmbH & Co.: Weinheim, 2007.

(6) Morse, J. W., In *Carbonates: Mineralogy and Chemistry*; Reeder, R. J., Eds.; BookCrafters, Inc.: Chelsea, MI, 1983; Vol. *11*, pp 227−264.

(7) Davis, J. A.; Fuller, C. C.; Cook, A. D. *Geochim. Cosmochim. Acta* **1987**, *51* (6), 1477−1490.

(8) Zachara, J. M.; Cowan, C. E.; Resch, C. T. *Geochim. Cosmochim. Acta* **1991**, *55* (6), 1549−1562.

(9) Stipp, S. L.; Hochella, M. F.; Parks, G. A.; Leckie, J. O. *Geochim. Cosmochim. Acta* **1992**, *56* (5), 1941−1954.

(10) Reeder, R. J. *Geochim. Cosmochim. Acta* **1996**, *60* (9), 1543−1552.

(11) Tesoriero, A. J.; Pankow, J. F. *Geochim. Cosmochim. Acta* **1996**, *60* (6), 1053−1063.

(12) Rimstidt, J. D.; Balog, A.; Webb, J. *Geochim. Cosmochim. Acta* **1998**, *62* (11), 1851−1863.

(13) Curti, E. *Appl. Geochem.* **1999**, *14* (4), 433−445.




DOI: 10.1021/acs.cgd.6b00536
*Cryst. Growth Des.* 2016, 16, 6199−6207

(14) Reeder, R. J.; Nugent, M.; Tait, C. D.; Morris, D. E.; Heald, S. M.; Beck, K. M.; Hess, W. P.; Lanzirotti, A. *Geochim. Cosmochim. Acta* **2001**, *65* (20), 3491−3503.
(15) Lakshtanov, L. Z.; Stipp, S. L. S. *Geochim. Cosmochim. Acta* **2004**, *68* (4), 819−827.
(16) Turner, B. D.; Binning, P.; Stipp, S. L. S. *Environ. Sci. Technol.* **2005**, *39* (24), 9561−9568.
(17) Renard, F.; Montes-Hernandez, G.; Ruiz-Agudo, E.; Putnis, C. V. *Chem. Geol.* **2013**, *340*, 151−161.
(18) Reeder, R. J. In *Carbonates: Mineralogy and Chemistry*, Reeder, R. J., Eds.; Mineralogical Society of America: Chelsea, MI, 1983; Vol. *11*, pp 1−48.
(19) Harstad, A. O.; Stipp, S. L. S. *Geochim. Cosmochim. Acta* **2007**, *71* (1), 56−70.
(20) Sand, K. K.; Rodriguez-Blanco, J. D.; Makovicky, E.; Benning, L. G.; Stipp, S. L. S. *Cryst. Growth Des.* **2012**, *12* (2), 842−853.
(21) Rodriguez-Blanco, J. D.; Sand, K. K.; Benning, L. G.: ACC and vaterite as metastable intermediates in the solution based crystallization of $CaCO_3$, In *New Perspectives on Mineral Nucleation and Growth*; van Driessche, A.; Kellermeier, M.; Benning, L. G., Eds.; Springer: Berlin, DOI: 10.1007/978-3-319-45669-0, in press.
(22) Montanari, G.; Lakshtanov, L. Z.; Tobler, D. J.; Dideriksen, K.; Dalby, K. N.; Bovet, N.; Stipp, S. L. S. *Cryst. Growth Des.* **2016**, *16* (9), 4813−4821.
(23) Sand, K. K.; Pedersen, C. S.; Sjoberg, S.; Nielsen, J. W.; Makovicky, E.; Stipp, S. L. S. *Cryst. Growth Des.* **2014**, *14* (11), 5486−5494.
(24) Stipp, S. L. S.; Lakshtanov, L. Z.; Jensen, J. T.; Baker, J. A. *J. Contam. Hydrol.* **2003**, *61* (1−4), 33−43.
(25) Lakshtanov, L. Z.; Stipp, S. L. S. *Geochim. Cosmochim. Acta* **2010**, *74* (9), 2655−2664.
(26) Strand, S.; Hognesen, E. J.; Austad, T. *Colloids Surf., A* **2006**, *275* (1−3), 1−10.
(27) Zhang, P. M.; Tweheyo, M. T.; Austad, T. *Colloids Surf., A* **2007**, *301* (1−3), 199−208.
(28) Austad, T.; Strand, S.; Madland, M. V.; Puntervold, T.; Korsnes, R. I. *SPE Reservoir Eval. Eng.* **2008**, *11* (4), 648−654.
(29) Sakuma, H.; Andersson, M. P.; Bechgaard, K.; Stipp, S. L. S. *J. Phys. Chem. C* **2014**, *118* (6), 3078−3087.
(30) Lager, A.; Webb, K. J.; Collins, I. R.; Richmond, D. M. LoSal Enhanced Oil Recovery: Evidence of Enhanced Oil Recovery at the Reservoir Scale, SPE Improved Oil Recovery Symposium, April 20−23, 2008, Tulsa, OK, Society of Petroleum Engineers: Richardson, TX.
(31) Austad, T.; Rezaeidoust, A.; Puntervold, T. Chemical Mechanism of Low Salinity Water Flooding in Sandstone Reservoirs, SPE Improved Oil Recovery Symposium, April 24−28, 2010, Tulsa, OK, Society of Petroleum Engineers: Richardson, TX.
(32) Shariatpanahi, S. F.; Strand, S.; Austad, T. *Energy Fuels* **2011**, *25* (7), 3021−3028.
(33) Matthiesen, J.; Bovet, N.; Hilner, E.; Andersson, M.; Schmidt, D.; Webb, K. J.; Dalby, K. N.; Hassenkam, T.; Crouch, J.; Collins, I. R.; Stipp, S. L. S. *Energy Fuels* **2014**, *28*, 4849−4858.
(34) Hassenkam, T.; Andersson, M.; Hilner, E.; Matthiesen, J.; Dobberschutz, S.; Dalby, K. N.; Bovet, N.; Stipp, S. L. S.; Salino, P.; Reddick, C.; Collins, I. R. *SPE J.* **2015**, DOI: 10.2118/169136-PA.
(35) Hilner, E.; Andersson, M. P.; Hassenkam, T.; Matthiesen, J.; Salino, P. A.; Stipp, S. L. S. *Sci. Rep.* **2015**, *5*, 9933.
(36) Berner, R. A. *Geochim. Cosmochim. Acta* **1975**, *39* (4), 489−494.
(37) Reddy, M. M.; Nancollas, G. H. *J. Cryst. Growth* **1976**, *35* (1), 33−38.
(38) Sjöberg, E. L. *Stockholm Contrib. Geol.* **1978**, *32*, 1−96.
(39) Busenberg, E.; Niel Plummer, L. N. *Geochim. Cosmochim. Acta* **1985**, *49* (3), 713−725.
(40) Mejri, W.; Korchef, A.; Tlili, M.; Ben Amor, M. *Desalin. Water Treat.* **2014**, *52* (25−27), 4863−4870.
(41) Mucci, A.; Morse, J. W. *Geochim. Cosmochim. Acta* **1983**, *47* (2), 217−233.
(42) Kralj, D.; Kontrec, J.; Brecevic, L.; Falini, G.; Nothig-Laslo, V. *Chem. - Eur. J.* **2004**, *10* (7), 1647−56.
(43) Pedersen, N. R.; Hassenkam, T.; Ceccato, M.; Dalby, K. N.; Mogensen, K.; Stipp, S. L. S. *Energy Fuels* **2016**, *30* (5), 3768−3775.
(44) Reddy, M. M.; Wang, K. K. *J. Cryst. Growth* **1980**, *50* (2), 470−480.
(45) Meyer, H. J. *J. Cryst. Growth* **1984**, *66* (3), 639−646.
(46) Saldi, G. D.; Jordan, G.; Schott, J.; Oelkers, E. H. *Geochim. Cosmochim. Acta* **2009**, *73* (19), 5646−5657.
(47) Di Tommaso, D.; de Leeuw, N. H. *Phys. Chem. Chem. Phys.* **2010**, *12* (4), 894−901.
(48) Chave, K. E. *J. Geol.* **1954**, *62* (3), 266−283.
(49) Nürnberg, D.; Bijma, J.; Hemleben, C. *Geochim. Cosmochim. Acta* **1996**, *60* (5), 803−814.
(50) Guilderson, T. P.; Pak, D. K. In *Encyclopedia of Quaternary Science*; Elias, S. A., Eds.; Elsevier: Amsterdam, 2007; pp 1766−1775.
(51) Gledhill, D. K.; Morse, J. W. *Geochim. Cosmochim. Acta* **2006**, *70* (23), 5802−5813.
(52) Mucci, A.; Canuel, R.; Zhong, S. J. *Chem. Geol.* **1989**, *74* (3−4), 309−320.
(53) Waly, T.; Kennedy, M. D.; Witkamp, G. J.; Amy, G.; Schippers, J. C. *Desalination* **2012**, *284*, 279−287.
(54) Titiloye, J. O.; Parker, S. C.; Mann, S. *J. Cryst. Growth* **1993**, *131* (3−4), 533−545.
(55) Prieto, M.; Putnis, A.; Fernandezdiaz, L.; Lopezandres, S. *J. Cryst. Growth* **1994**, *142* (1−2), 225−235.
(56) Falini, G.; Fermani, S.; Tosi, G.; Dinelli, E. *Cryst. Growth Des.* **2009**, *9* (5), 2065−2072.
(57) Stipp, S. L.; Hochella, M. F. *Geochim. Cosmochim. Acta* **1991**, *55* (6), 1723−1736.
(58) Lakshtanov, L. Z.; Bovet, N.; Stipp, S. L. S. *Geochim. Cosmochim. Acta* **2011**, *75* (14), 3945−3955.
(59) Parkhurst, D. L. *A Computer Program for Speciation, Reaction-Path, Advective-Transport, and Inverse Geochemical Calculations*; U.S. Geological Survey: Lakewood, CO, 1995.
(60) Plummer, L. N.; Busenberg, E. *Geochim. Cosmochim. Acta* **1982**, *46* (6), 1011−1040.
(61) Keller, K. S.; Olsson, M. H. M.; Yang, M.; Stipp, S. L. S. *Langmuir* **2015**, *31* (13), 3847−3853.
(62) Stipp, S. L. S.; Eggleston, C. M.; Nielsen, B. S. *Geochim. Cosmochim. Acta* **1994**, *58* (14), 3023−3033.
(63) Arvidson, R. S.; Mackenzie, F. T. *Am. J. Sci.* **1999**, *299* (4), 257−288.
(64) Patterson, A. L. *Phys. Rev.* **1939**, *56* (10), 978−982.
(65) Coelho, A. A. *J. Appl. Crystallogr.* **2003**, *36*, 86−95.
(66) Amjad, Z. *Langmuir* **1987**, *3* (6), 1063−1069.
(67) Takano, B. *Chem. Geol.* **1985**, *49* (4), 393−403.
(68) Staudt, W. J.; Reeder, R. J.; Schoonen, M. A. A. *Geochim. Cosmochim. Acta* **1994**, *58* (9), 2087−2098.
(69) Pingitore, N. E.; Meitzner, G.; Love, K. M. *Geochim. Cosmochim. Acta* **1995**, *59* (12), 2477−2483.
(70) Grossman, E. L.; Mii, H. S.; Zhang, C. L.; Yancey, T. E. *J. Sediment. Res.* **1996**, *66* (5), 1011−1022.
(71) Kontrec, J.; Kralj, D.; Brecevic, L.; Falini, G.; Fermani, S.; Noethig-Laslo, V.; Mirosavljevic, K. *Eur. J. Inorg. Chem.* **2004**, *2004*, 4579−4585.
(72) Hochella, M. F. In *Spectroscopic Methods in Mineralogy and Geology*; Hawthorne, F. C., Eds.; Mineralogical Society of America: Washington, D.C., 1988; Vol. *18*, pp 572−638.
(73) Hillner, P. E.; Gratz, A. J.; Manne, S.; Hansma, P. K. *Geology* **1992**, *20* (4), 359−362.
(74) Fernandez-Diaz, L.; Putnis, A.; Prieto, M.; Putnis, C. V. *J. Sediment. Res.* **1996**, *66* (3), 482−491.
(75) Zhang, Y. P.; Dawe, R. A. *Chem. Geol.* **2000**, *163* (1−4), 129−138.
(76) Arvidson, R. S.; Collier, M.; Davis, K. J.; Vinson, M. D.; Amonette, J. E.; Luttge, A. *Geochim. Cosmochim. Acta* **2006**, *70* (3), 583−594.
(77) Astilleros, J. M.; Fernandez-Diaz, L.; Putnis, A. *Chem. Geol.* **2010**, *271* (1−2), 52−58.


DOI: 10.1021/acs.cgd.6b00536
*Cryst. Growth Des.* 2016, 16, 6199−6207

(78) Kerisit, S.; Parker, S. C. *J. Am. Chem. Soc.* **2004**, *126* (32), 10152−10161.



DOI: 10.1021/acs.cgd.6b00536
*Cryst. Growth Des.* 2016, 16, 6199−6207